Journal of MATERIALS RESEARCH

Article
DOI: 10.1557/jmr.2019.290

Bilayer graphene-covered Cu flexible electrode with excellent mechanical reliability and electrical performance

Yu-Jia Yang[1], Bin Zhang[1,a], Hong-Yuan Wan[2], Kun Liu[3], Guang-Ping Zhang[4]

[1]Key Laboratory for Anisotropy and Texture of Materials, Ministry of Education, School of Materials Science and Engineering, Northeastern University, Shenyang 110819, People's Republic of China
[2]Shenyang National Laboratory for Materials Science, Institute of Metal Research, Chinese Academy of Sciences, Shenyang 110016, People's Republic of China; and School of Materials Science and Engineering, University of Science and Technology of China, Shenyang 110016, People's Republic of China
[3]School of Mechanical Engineering and Automation, Northeastern University, Shenyang 110819, People's Republic of China
[4]Shenyang National Laboratory for Materials Science, Institute of Metal Research, Chinese Academy of Sciences, Shenyang 110016, People's Republic of China
[a]Address all correspondence to this author. e-mail: zhangb@atm.neu.edu.cn

Received: 2 August 2019; accepted: 3 September 2019

Flexible electrode is an indispensable component of emerging portable, flexible, and wearable electronic devices. Although various flexible electrodes with different dimensions and functions have been explored, developing a new electrode material with excellent mechanical reliability and superior electrical performance remains a challenge. Here, a graphene-covered Cu composite electrode film with a total thickness of ~100 nm is successfully fabricated onto a flexible polyimide substrate by means of a series of assembly methods including physical vapor deposition, chemical vapor deposition, and transfer technique. The composite electrode film on the flexible substrate exhibits evidently enhanced tensile strength, monotonic bending, and repeatedly bending fatigue reliability as well as electrical performance compared with that of the bared Cu film electrode. Such excellent mechanical performances are attributed to the role of the graphene coating in suppressing fatigue damage formation and preventing crack advance. It is expected that the chemical vapor-deposited graphene-covered Cu composite electrode would extend the potential ultrathin metal film electrode as the innovative electrode material for the next-generation flexible electronic devices.

Introduction

Flexible electrode is an essential component of various recently emerging portable, flexible, and wearable electronic devices such as flexible energy storage devices, flexible displays, wearable sensor system, and implantable medical devices [1, 2, 3, 4, 5, 6, 7, 8, 9, 10, 11]. In many cases, the major limitation for the development flexible electrode materials with superior performance is their long-term service reliability since the flexible devices are inevitably subjected to cyclic stretching, repeatedly bending, or even twisting in their daily use. One effective solution is to utilize robust materials for optimizing their performance and long-term service reliability [12].

Recently, carbon nanotubes (CNT) [13, 14, 15], reduced graphene oxide (rGO) [16, 17], carbon cloth [18, 19, 20], conductive paper (cellulose) [21, 22], low-dimensional nanostructured transition metal dichalcogenides [7, 23] and ultrathin metal films [24, 25, 26, 27], as well as their composites [28, 29, 30, 31] have been utilized to replace the conventional indium tin oxide (ITO) material, which is so brittle that not suitable for the flexible electrodes [32]. Due to the large contact resistance of tube–tube junctions, a CNT network is still far from practical applications [27]. One of the potential alternatives is metal (i.e., Au, Ag, and Cu)-based nanostructures in the form of either a ultrathin continuous film (dozens or hundreds of nanometer thickness) or a nanowire network supported by flexible polymer substrates [27, 33]. Ultrathin Cu film is one of the most widely used metallic interconnect/electrodes in the devices due to its relatively low cost and high electrical conductivity. The yield strength of the Cu film was improved by 1000 MPa, from ~300 to ~1300 MPa, by tailoring microstructure, such as the film thickness and the grain size [34]. In addition, fatigue cracking resistance was enhanced to some extent by annealing but still not fully satisfied [26, 35]. A key question is how to further improve

https://doi.org/10.1557/jmr.2019.290 Published online by Cambridge University Press

© Materials Research Society 2019

the long-term mechanical reliability and stability without loss of electrical conductivity. Liu et al. found that the layer interface of laminated composites can delay the premature of local necking of the constituent layers, resulting in a significant enhancement in the tensile ductility [36]. Therefore, one of the possible approaches to fabricate ultrathin metal films with high-fatigue performance is to strongly constrain and delay the formation of fatigue damage of the metal film by introducing a heterogeneous interface.

Graphene with a honeycomb lattice, that combines remarkable mechanical properties (yield strength is 130 GPa and Young's modulus is 1 TPa), high electrical conductivity [the electron mobility is 2×10^5 cm^2/(V s) and the minimum sheet resistance of an ideal undoped monolayer graphene is 31 Ω/sq.], and thermal conductivity (~5300 W/m K), is a unique electrode material as well [12, 37, 38, 39]. In particular, the integration of graphene and ultrathin metal film enables the mechanical properties of the graphene/metal composites largely improved without loss of electrical conductivity [40, 41, 42, 43, 44, 45, 46, 47]. Therefore, considerable amount of research has been conducted on fabrication the graphene/metal composites, including electrodeposition [40, 48], molecule-level mixing [42, 43, 45], ball milling [47, 49, 50] followed by spark plasma sintering [42, 43, 44, 45, 46] and/or high-ratio differential speed rolling [47], and hot-pressing [41] after chemical vapor deposition (CVD) methods. Several technical challenges such as controlling the layer numbers and the quality of rGO mixed in the composites are critical during the fabrication process. Due to extreme high temperature (~1000 °C) during the CVD process, large-area and high-quality monolayer or multilayer graphene needs to be firstly grown on Cu foils and then transferred onto the Cu/PI by wet etching transfer technique [51], which paves a road for fabricating flexible metal electrode coated with controllable layers of graphene [12, 38]. So far, the durability of these flexible devices is only calculated by measuring the electrical resistivity or resistance evolution after the electrode was bent at a certain curvature for 10^3–10^6 cycles [12, 29]. In fact, cracks may initiate as the electrical resistance imperceptibly increases and then gradually propagate with fatigue cycle increasing. Thus, the critical strain amplitude for fatigue crack initiation needs to be determined. What is more, to further improve the mechanical reliability of the flexible electrodes under cyclic loading, the mechanism for the graphene delaying the fatigue damage formation of covered metal films is urgently needs to be clarified.

In this work, we fabricated a graphene-covered Cu (GC-Cu) composite electrode with a thickness of 100 nm on a polyimide (PI) substrate by means of a series of methods including physical vapor deposition (PVD), CVD, and transfer techniques. A series of detailed processes of the deposition of the Cu film on the PI substrate, the growth of graphene on the Cu foil by CVD, and subsequent transfer of the CVD graphene onto the as-deposited Cu film were depicted in Fig. 1. Raman spectroscopy was used to characterize the GC-Cu composite electrode film. Compared with the bared Cu (B-Cu) film, the mechanical properties of the prepared GC-Cu composite film, such as tensile, monotonic bending, and repeatedly bending fatigue properties, were enhanced. Meanwhile, the electrical properties of the GC-Cu composite film during the mechanical loading were also superior to that of the B-Cu counterpart. Furthermore, the role of graphene in delaying the fatigue damage formation of the GC-Cu composite film subjected to mechanical loading was discussed. It is expected that such investigation would further promote the nature of wearable application technologies.

Results and discussion

Microstructures

Figure 2(a) shows that the as-deposited B-Cu film is clean and even without any impurities or defects. Figure 2(b) shows

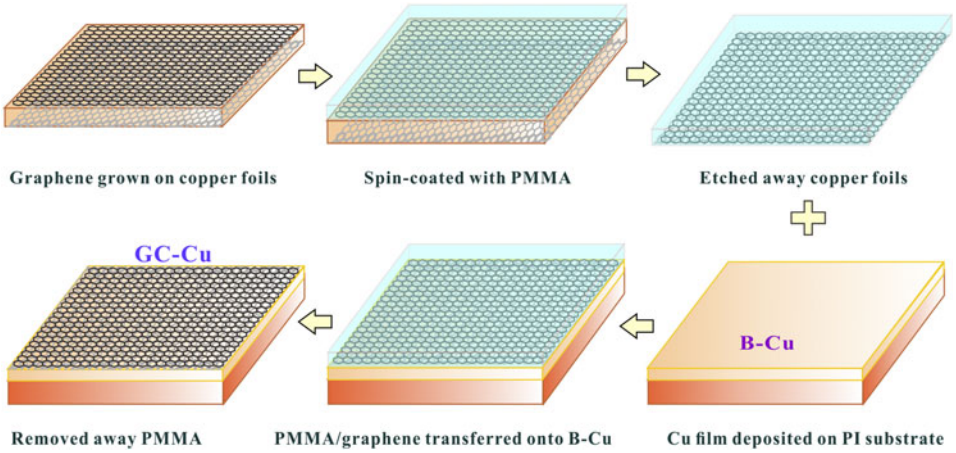


Figure 1: Schematic illustration of fabricating process of a bilayer CVD graphene covered on the surface of a Cu film.

https://doi.org/10.1557/jmr.2019.290 Published online by Cambridge University Press

© Materials Research Society 2019

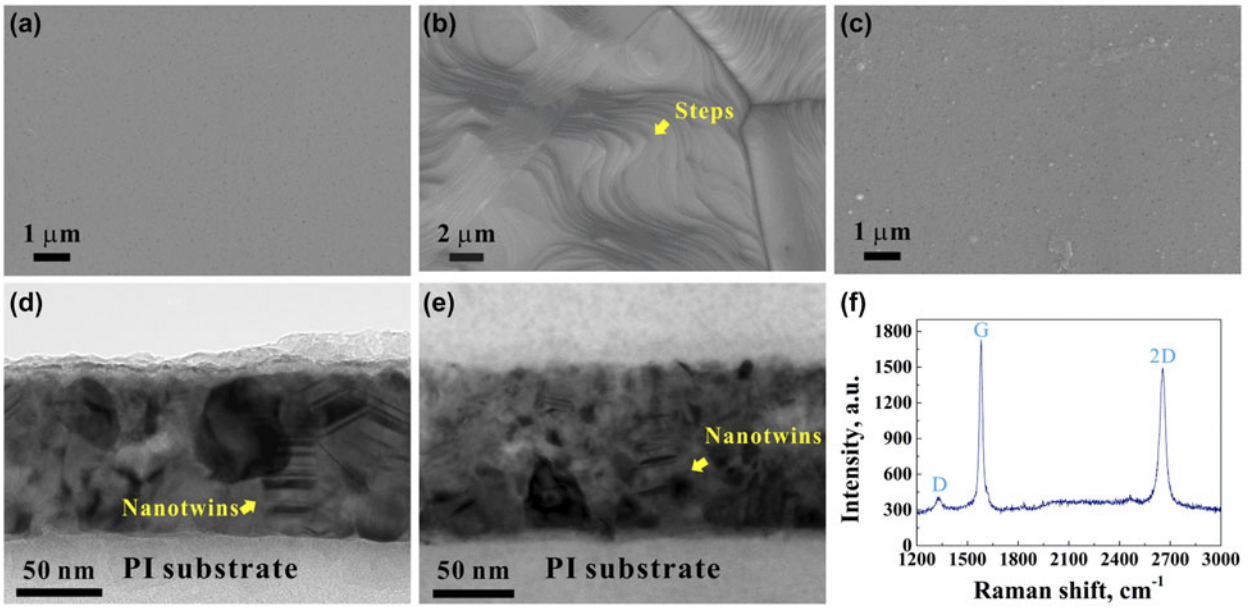


Figure 2: SEM morphologies of (a) B-Cu films deposited by PVD, the surface is clean and even without any impurities or defects. (b) Graphene on Cu by CVD, Cu surface steps and grain boundaries can be clearly observed. (c) GC-Cu films obtained by transfer graphene onto B-Cu films, high-quality graphene has been successfully transferred onto the B-Cu films without any cracks. Cross-sectional TEM view of (d) B-Cu films, (e) GC-Cu films, and (f) Raman spectrum of the GC-Cu films.

a typical SEM image of the CVD graphene grown on the surface of the Cu foil. Steps and grain boundaries of the Cu foil can be clearly observed, indicating that the graphene grown on the Cu foil surface is continuous and completely covers the Cu foil [52]. Morphology of the GC-Cu composite film shown in Fig. 2(c) reveals that the high-quality graphene has been successfully transferred onto the as-deposited Cu film without any macrocracks.

TEM cross-sectional observations of the B-Cu film [Fig. 2(d)] and the GC-Cu composite film [Fig. 2(e)] show that the thicknesses of both the B-Cu and the GC-Cu films are the same ~100 nm. The grain size of the Cu film is in a range of 20–50 nm, and some nanotwins appeared in the as-deposited Cu film. Since the graphene grown on the Cu foil is a self-limited process and the graphene coverage is nearly 100% monolayer [53], the graphene grown on both sides of the copper foil substrate was transferred onto the Cu film to remedy the damage of monolayer graphene and ensure the Cu film fully covered by graphene, as schematically illustrated in Fig. 1. Thus, bilayer graphene was transferred onto the as-deposited Cu films. The Raman spectra of the GC-Cu films confirm the typical graphene feature characterized by the D band position of 1329 cm^{-1}, G band position of 1581 cm^{-1}, and 2D band position of 2656 cm^{-1} [see Fig. 2(f)]. The intensity ratio of the G peak to the 2D peak (I_G/I_{2D}) is ~1.67, and the full width at half-maximum of the 2D peak is ~51 cm^{-1}, indicating that the graphene film is bilayer [54, 55].

Tensile properties

Figure 3(a) presents the load–strain curves of PI substrates, the B-Cu films, and GC-Cu composite films. The tensile stress (σ) of the B-Cu and the GC-Cu films on the PI substrate was calculated by

$$\sigma = \frac{1}{hw}(F_{\text{total}} - F_{\text{PI}}) \quad , \tag{1}$$

where F_{total} is the force acting on the entire specimen including the PI substrate and the surface coating, F_{PI} is the force on the PI substrate, w and h represent the gauge width and thickness of the specimens, respectively. The stress–strain curves of the B-Cu and the GC-Cu are thereby obtained based on Eq. (1) and shown in Figs. 3(b) and 3(c), respectively. The yield stress ($\sigma_{0.2}$) of the GC-Cu film (~1940 MPa) was enhanced by ~47% compared with that of the B-Cu film (~1320 MPa), due to the bilayer graphene covering. Ultimate tensile strengths (σ_t) of the B-Cu and GC-Cu films are ~1375 MPa and ~2359 MPa, respectively. It is generally accepted that the graphene reinforces metal matrix through four typical strengthening mechanisms, load transfer strengthening, grain refinement, thermal mismatch strengthening, and Orowan strengthening [56]. For GC-Cu film presented in this work, load transfer is the most important strengthening mechanism benefited from the graphene/Cu interface [57, 58]. The graphene effectively blocks the dislocations from penetrating through the graphene/Cu interface, and loads can be transferred to the graphene layer during the tensile process [38, 59]. The dislocation sliding was

https://doi.org/10.1557/jmr.2019.290 Published online by Cambridge University Press

© Materials Research Society 2019

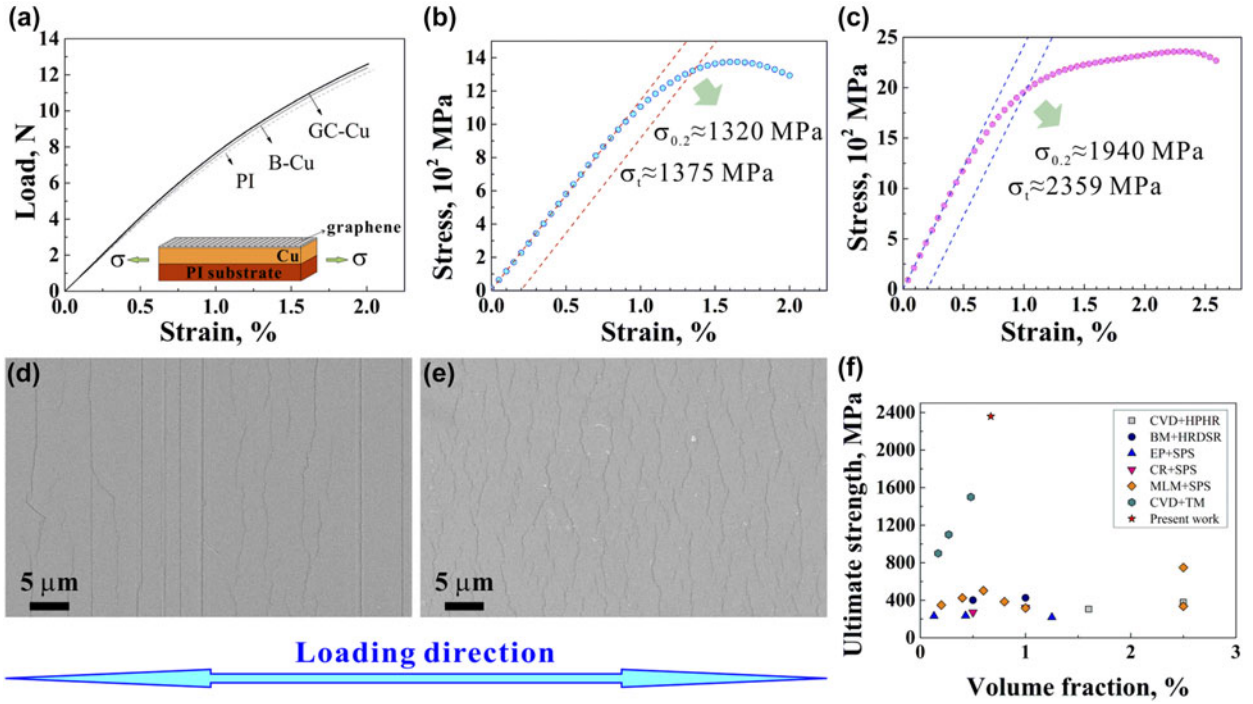


Figure 3: (a) Load–strain curves of PI substrate, B-Cu film and GC-Cu film; stress–strain curves of (b) a B-Cu film and (c) a GC-Cu film; SEM images of tensile cracks of (d) a B-Cu film and (e) a GC-Cu film under ~11% applied strain; (f) a comparison of the ultimate tensile strengths of our GC-Cu films with those of the others reports, graphene-reinforced Cu matrix composites as a function of reinforcement amount of graphene, including CVD + HPHR [41], BM + HRDSR [47], EP + SPS [44], CR + SPS [46], MLM + SPS [42, 43, 45], and CVD + transfer method (TM, strength measured by nanopillar compression testing) [38].

prevented and dislocations piled up at the interface under tensile loading [38, 58, 60]. What's more, the shear modulus and the lattice parameters mismatches between Cu and graphene may reduce the possibility of dislocations in copper slipping out of the surface, leading to the enhancement of strength for GC-Cu film [60, 61].

Such a strengthening effect of the GC-Cu films was also verified by SEM observation of crack morphologies shown in Figs. 3(d) and 3(e) comparatively. Since the transmittance of graphene is 97.7% [62], crack morphologies of Cu films can be identified clearly from the SEM image even though the surface is coated by bilayer graphene. Figure 3(d) shows that long and straight cracks on the B-Cu films appeared on the specimen surface, while Fig. 3(e) indicates that zigzag cracks appeared on the GC-Cu films, which are much shorter than the straight ones in the B-Cu films, implying that cracking resistance was enhanced owing to the graphene covering on the Cu film surface. Figure 3(f) presents a comparison of σ_t between the present GC-Cu film and the graphene-reinforced Cu matrix composites fabricated by other methods [38, 41, 42, 43, 44, 45, 46, 47]. It is found that the strengthening extent of the present GC-Cu composite film is evidently higher than those of the other traditional rGO-reinforced Cu matrix composites [41, 42, 43, 44, 45, 46, 47] and also superior to that of nanolayered composite consisting of alternating layers of Cu and monolayer graphene [38]. Thus, the present Cu films covered by high-quality bilayer graphene possess the highest ultimate tensile strength, which would be of great potential for high-performance stretchable devices.

Bending properties

To examine the electrical properties of the GC-Cu composite electrodes subjected to mechanical bending, the simply supported beam bending test was conducted on home-made apparatus [63, 64] with simultaneously measuring the real-time electrical resistance (R) of the films as the applied bending strain (ε) increased from 0 to 1.64%. A relative resistance change $\left(\tilde{R} = \frac{R-R_0}{R_0}\right)$ of the B-Cu films and GC-Cu films as a function of ε are shown in Fig. 4(a), which can be divided into two stages. In the first stage, $\tilde{R}$ of the B-Cu films slightly increases, while that of the GC-Cu films basically remains invariable. The main reason is that the GC-Cu film has a higher elastic modulus and yield strength, resulting in a delay of yielding compared with the B-Cu films with lower elastic modulus and yield strength. In the second stage, both the B-Cu and GC-Cu specimens have an evident increase in $\tilde{R}$ due to the formation of damage. However, the increase rate of the GC-Cu film is lower than that of the B-Cu film, indicating that the coated graphene of the GC-Cu films can effectively resist the

https://doi.org/10.1557/jmr.2019.290 Published online by Cambridge University Press

© Materials Research Society 2019

evolution of damage with the increase in bending strain [65]. Unexpectedly, the fitted lines of these two stages for B-Cu films and GC-Cu films almost intercepted at the same strain (~1.3%), which may be due to the weak interface bonding between graphene and Cu [57, 66]. It is believed that the damage formation of the films would be further delayed if the adhesion of the graphene/Cu interface had been improved through optimizing graphene transfer method.

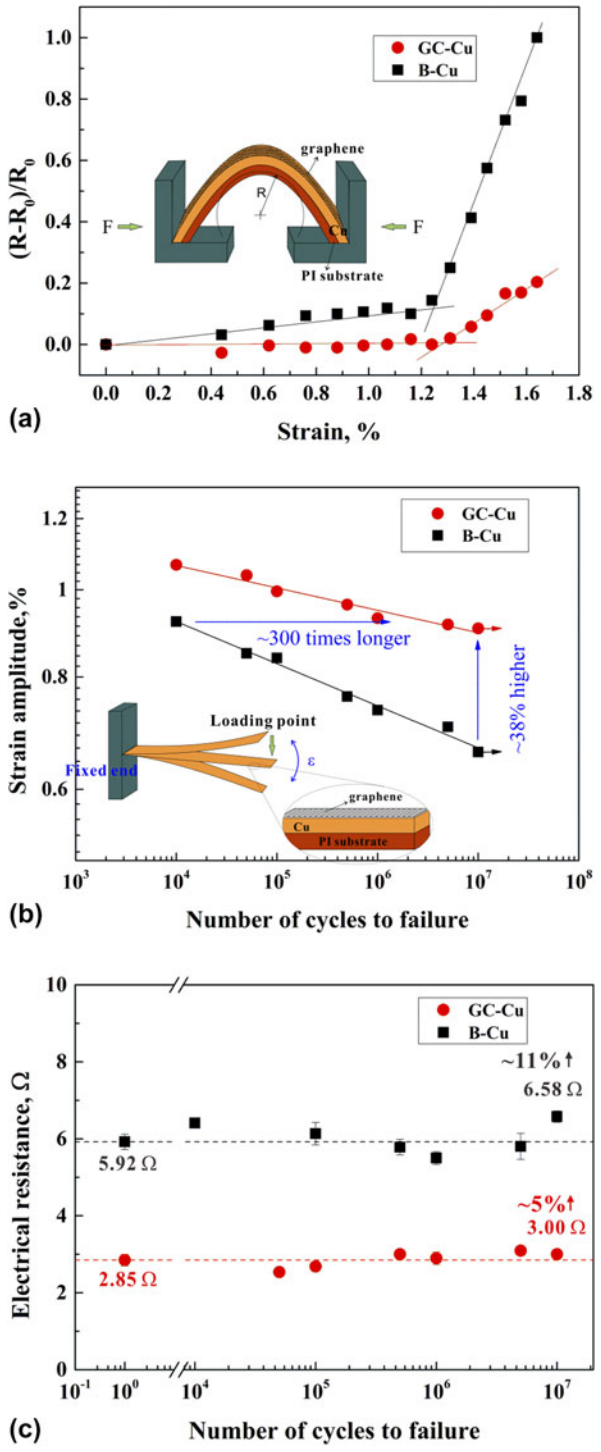


Figure 4: (a) Normalized resistance change curves versus applied strain of B-Cu films and GC-Cu films under bending tests; (b) S–N curves of the applied strain amplitudes versus numbers of cycles to failure of B-Cu films and GC-Cu films under cyclic bending loads; (c) Electrical resistance of the B-Cu and GC-Cu films before and after cyclic bending tests.

Bending fatigue properties

Typical relationship between the applied strain amplitude ($\Delta\varepsilon/2$) and the fatigue life (N_f) for B-Cu and GC-Cu films is presented in Fig. 4(b). It is clear that the fatigue life of the GC-Cu films was enhanced by ~300 times compared to the B-Cu films. Especially the critical fatigue strain amplitudes corresponding to the lowest strain amplitudes for fatigue cracking (0.91% for GC-Cu films) is ~38% higher than that of the B-Cu ones (0.66%). Moreover, besides great improvement in the fatigue strength, a simultaneous enhancement of conductivity during bending fatigue is shown in Fig. 4(c). Initial resistances of the as-prepared B-Cu and the GC-Cu films are 5.92 Ω and 2.85 Ω, respectively, as indicated by dash lines in Fig. 4(c). After 10^7-cycle bending tests, the resistance of the B-Cu films increased by ~11% (6.58 Ω), while that of the GC-Cu films only increased by ~5% (3.00 Ω). Furthermore, the less increase in the GC-Cu film resistance indicates that fatigue cracks would not form in the films and the electrical performance of the films would not be weakened if the GC-Cu films were subjected to the strain amplitude less than 0.91% and even for over 10^7 cycles.

Figure 5(a)–5(d) present SEM images of fatigue cracking behavior of the B-Cu films and GC-Cu ones after repeatedly bending at $\Delta\varepsilon/2 = 0.96\%$ for 10^6 cycles, respectively. Some parallel, long, straight fatigue cracks and some unbroken traces before the crack initiation in the same direction were observed on the B-Cu film [see Figs. 5(a) and 5(b)], while for the GC-Cu

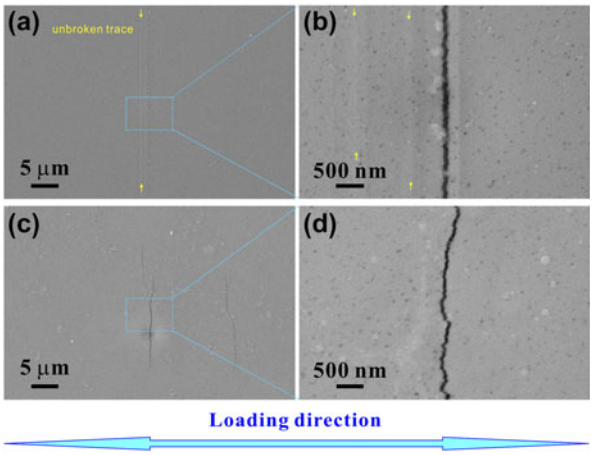


Figure 5: SEM images of bending fatigue cracks of (a) and (b) B-Cu films, and (c) and (d) GC-Cu films after 10^6 cycle loading, the strain amplitude is 0.96%.

https://doi.org/10.1557/jmr.2019.290 Published online by Cambridge University Press

© Materials Research Society 2019

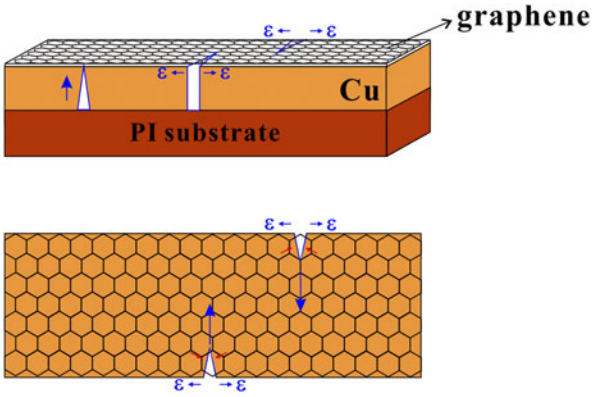


Figure 6: Schematic illustration of cracks propagation in GC-Cu films under cyclic bending tests.

film, the formation of shorter and fewer zigzag cracks [see Figs. 5(c) and 5(d)] indicates that the crack propagation was prevented by the transferred graphene on the surface of the GC-Cu film. The fact that cracks in the GC-Cu films became more tortuous than that in the B-Cu ones at $\Delta\varepsilon/2 = 0.96\%$ demonstrates that the crack propagation resistance is effectively enhanced by graphene coated on Cu films.

It is well accepted that the fatigue life is composed of crack initiation life and crack propagation life. In the fatigue crack initiation stage, the coated graphene of GC-Cu films with higher yield strength acted as a barrier impeding the formation of extrusions of the Cu film, which can effectively resist the crack initiation. In the fatigue crack propagation stage, once cracks began to propagate in the Cu film of the GC-Cu films, the as-coated graphene still subjected to elastic deformation due to the ultrahigh elastic modulus, which would produce an opposite force to resist the crack opening in the Cu layer, as shown in Fig. 6. This means that the locally high stress at the crack tip was somewhat screened by the graphene layer and a part of the energy driving crack propagation was absorbed by the coated graphene on the Cu films. Thus, the crack propagation distance of the GC-Cu films became shorter than that of the B-Cu ones when the same strain amplitude was applied. Fatigue cracks initiated from the Cu layer then stopped by the graphene interface has also been confirmed by Hwang et al. with cross-sectional SEM and TEM observations [12]. And also, the graphene/Cu interface with strong sp^2 bonding can act as an effective barrier for deflecting the fatigue cracks under cyclic bending [12, 38]. This is the reason for the GC-Cu films with longer fatigue life and higher fatigue limit than that of the B-Cu ones. The present finding not only provides a potential candidate for high-performance electrodes of the flexible devices but also reveals a new idea to design strong composites by employing graphene to suppress the formation and development of mechanical damage.

Conclusion

Enhanced by surface-covered bilayer graphene, the yield strength of the GC-Cu composite film is evidently enhanced by 47%, from ~1320 MPa for the B-Cu films to ~1940 MPa, and the ultimate tensile strength of the GC-Cu films is improved by 72% (from ~1375 to ~2359 MPa). The critical strain for fatigue crack initiation of the B-Cu and GC-Cu films was determined as ~1.3%. The critical fatigue strain amplitude corresponding to the lowest strain amplitude for bending fatigue cracking of the GC-Cu films is improved from 0.66 to 0.91%, while the electric resistance of the GC-Cu films only increased by ~5% after 10^7-cycle bending fatigue. It demonstrates that the bilayer graphene-covered Cu films on a PI substrate have a good combination of high electrical performance and excellent durability against mechanical deformation.

Experimental

Fabrication of B-Cu films

Cu films (target purity: 99.99%) with thickness of ~100 nm were deposited onto a PI (Dupont®, Wilmington, Delaware, USA) substrate with dimensions of 40 mm × 40 mm × 125 μm by radio frequency magnetron sputtering (JGP 560 high-vacuum magnetron sputtering system) under ultra-high vacuum ($<10^{-3}$ Pa) with the working pressure of 0.5 Pa, the deposition rate was ~0.185 nm/s, and the flow rate of argon was 25 sccm. Prior to the deposition, the substrates were ultrasonically cleaned in ethanol and deionized water to remove the contamination.

Fabrication of GC-Cu composite films

High-quality graphene was grown on both sides of a copper foil (99.8%, Alfa-Aesar, Shanghai, China, Item No. 13382) and then transferred onto the B-Cu film to make sure the Cu film is fully covered by graphene. The upper side surface of the graphene on the copper foil was spin-coated (4000 rpm × 40 s) with a layer of poly-methyl methacrylate (PMMA) (MW 350,000; 46 mg/mL in chlorobenzene) [52, 67]. Edges of the specimen were cut by a sharp knife to make sure the copper foil in the middle layer exposed outside. The copper foil was etched away by dipping in an aqueous ammonium persulfate solution (0.1 M) after the PMMA cured. The PMMA-coated graphene was floated on the solution and rinsed several times by deionized water after the copper foil was completely dissolved. The PMMA/graphene was transferred onto the Cu film, and the specimen was dried in air for 30 min and then in vacuum drying chamber for 30 min to evaporate out the excess water between graphene and Cu. Subsequently, the PMMA coating was removed using acetone and the GC-Cu composite film was obtained.

https://doi.org/10.1557/jmr.2019.290 Published online by Cambridge University Press

© Materials Research Society 2019

Microstructure characterization

Surface morphologies of the B-Cu film, the GC-Cu film, and fatigue cracks of the samples after tensile or fatigue tests were observed by a field-emission scanning electron microscope (FE-SEM; Zeiss, Supra 35, Oberkochen, Germany). Cross-sectional view of the films was measured by a field-emission transmission electron microscope (FE-TEM; FEI, Tecnai 20, Hillsboro, Oregon). To evaluate the quality of transferred graphene, a Raman spectroscopy was measured with a XPLORA full-automatic Raman spectrometer with a laser wavelength of 638 nm and a 50× objective lens. Electrical resistance of the film was measured by a digital multimeter (Agilent 34410A, Keysight, Shenzhen, China) with a resolution of 10^{-3} Ω.

Tensile test

The tensile samples were cut into 16 mm in length and 2 mm in width, and the gauge length and the gauge width of the tensile specimen are 10 mm and 2 mm, respectively. Tensile tests were performed using a microforce testing system (MMT-101NV-10 SHIMADZU, Kyoto, Japan) with samples mounted on a template made of card-stock.

Monotonic bending test

The simply supported beam bending samples with a length of 16 mm and a width of 2 mm were prepared and then mounted on card-stocks. Monotonic bending tests were performed with measuring the real-time electrical resistance of the film simultaneously. The applied strain (ε) was calculated according to our previous report [68].

Repeatedly bending fatigue test

Cantilever beam-type specimens with a gauge length of 6 mm and gauge width of 2 mm were installed on a home-made system [69]. A constant deflection with 50 Hz loading frequency was applied to the free end of the specimens, inducing a bending curvature (κ) of ± 0.173. The strain (ε) applied to the samples can be calculated following the method reported previously [70].

Acknowledgments

This work was supported by the National Natural Science Foundation of China (NSFC, Grant Nos. 51671050, 51971060, and 51571199).

References

1. **D. Jia, D. Jiang, Y. Zheng, H. Tan, X. Cao, F. Liu, L. Yue, Y. Sun, and J. Liu**: Electrochemical synthesis of NiCo layered double hydroxide nanosheets decorated on moderately oxidized graphene films for energy storage. *Nanoscale* **11**, 2812 (2019).
2. **Y. Yu, Y. Luo, H. Wu, K. Jiang, Q. Li, S. Fan, J. Li, and J. Wang**: Ultrastretchable carbon nanotube composite electrodes for flexible lithium-ion batteries. *Nanoscale* **10**, 19972 (2018).
3. **L. Zhu, D. Zheng, Z. Wang, X. Zheng, P. Fang, J. Zhu, M. Yu, Y. Tong, and X. Lu**: A confinement strategy for stabilizing ZIF-derived bifunctional catalysts as a benchmark cathode of flexible all-solid-state zinc-air batteries. *Adv. Mater.* **30**, 1805268 (2018).
4. **Y. Yao, M. Chen, R. Xu, S. Zeng, H. Yang, S. Ye, F. Liu, X. Wu, and Y. Yu**: CNT interwoven nitrogen and oxygen dual-doped porous carbon nanosheets as free-standing electrodes for high-performance Na–Se and K–Se flexible batteries. *Adv. Mater.* **30**, 1805234 (2018).
5. **F-C. Liang, Y-W. Chang, C-C. Kuo, C-J. Cho, D-H. Jiang, F-C. Jhuang, S-P. Rwei, and R. Borsali**: A mechanically robust silver nanowire–polydimethylsiloxane electrode based on facile transfer printing techniques for wearable displays. *Nanoscale* **11**, 1520 (2019).
6. **J. Song, T. Fang, J. Li, L. Xu, F. Zhang, B. Han, Q. Shan, and H. Zeng**: Organic–inorganic hybrid passivation enables perovskite QLEDs with an EQE of 16.48%. *Adv. Mater.* **30**, 1805409 (2018).
7. **I.J. Park, T.I. Kim, S. Kang, G.W. Shim, Y. Woo, T.S. Kim, and S.Y. Choi**: Stretchable thin-film transistors with molybdenum disulfide channels and graphene electrodes. *Nanoscale* **10**, 16069 (2018).
8. **H.S. Jo, H-J. Kwon, T-G. Kim, C-W. Park, S. An, A.L. Yarin, and S.S. Yoon**: Wearable transparent thermal sensors and heaters based on metal-plated fibers and nanowires. *Nanoscale* **10**, 19825 (2018).
9. **A.K. Yetisen, J.L. Martinez-Hurtado, B. Ünal, A. Khademhosseini, and H. Butt**: Wearables in medicine. *Adv. Mater.* **30**, 1706910 (2018).
10. **T.P. Huynh and H. Haick**: Autonomous flexible sensors for health monitoring. *Adv. Mater.* **30**, 1802337 (2018).
11. **Z. Pu, J. Tu, R. Han, X. Zhang, J. Wu, C. Fang, H. Wu, X. Zhang, H. Yu, and D. Li**: A flexible enzyme-electrode sensor with cylindrical working electrode modified with a 3D nanostructure for implantable continuous glucose monitoring. *Lab Chip* **18**, 3570 (2018).
12. **B. Hwang, W. Kim, J. Kim, S. Lee, S. Lim, S. Kim, S.H. Oh, S. Ryu, and S.M. Han**: Role of graphene in reducing fatigue damage in Cu/Gr nanolayered composite. *Nano Lett.* **17**, 4740 (2017).
13. **S. Park, M. Vosguerichian, and Z. Bao**: A review of fabrication and applications of carbon nanotube film-based flexible electronics. *Nanoscale* **5**, 1727 (2013).
14. **L. Liu, L. Ding, D. Zhong, J. Han, S. Wang, Q. Meng, C. Qiu, X. Zhang, L-M. Peng, and Z. Zhang**: Carbon nanotube complementary gigahertz integrated circuits and their applications on wireless sensor interface systems. *ACS Nano* **13**, 2526 (2019).

https://doi.org/10.1557/jmr.2019.290 Published online by Cambridge University Press

© Materials Research Society 2019

15. **H. Zhang, L. Xiang, Y. Yang, M. Xiao, J. Han, L. Ding, Z. Zhang, Y. Hu, and L-M. Peng**: High-performance carbon nanotube complementary electronics and integrated sensor systems on ultrathin plastic foil. *ACS Nano* **12**, 2773 (2018).
16. **C. Li, M. Ding, B. Zhang, X. Qiao, and C.Y. Liu**: Graphene aerogels that withstand extreme compressive stress and strain. *Nanoscale* **10**, 18291 (2018).
17. **W.G. Chong, Y. Xiao, J-Q. Huang, S. Yao, J. Cui, L. Qin, C. Gao, and J-K. Kim**: Highly conductive porous graphene/sulfur composite ribbon electrodes for flexible lithium–sulfur batteries. *Nanoscale* **10**, 21132 (2018).
18. **Z. Deng, H. Jiang, Y. Hu, Y. Liu, L. Zhang, H. Liu, and C. Li**: 3D ordered macroporous MoS_2@C nanostructure for flexible Li-ion batteries. *Adv. Mater.* **29**, 1603020 (2017).
19. **C. Guan, A. Sumboja, H. Wu, W. Ren, X. Liu, H. Zhang, Z. Liu, C. Cheng, S.J. Pennycook, and J. Wang**: Hollow Co_3O_4 nanosphere embedded in carbon arrays for stable and flexible solid-state zinc-air batteries. *Adv. Mater.* **29**, 1704117 (2017).
20. **B. Liu, J. Zhang, X. Wang, G. Chen, D. Chen, C. Zhou, and G. Shen**: Hierarchical three-dimensional $ZnCo_2O_4$ nanowire arrays/carbon cloth anodes for a novel class of high-performance flexible lithium-ion batteries. *Nano Lett.* **12**, 3005 (2012).
21. **Y. Zhang, L. Zhang, K. Cui, S. Ge, X. Cheng, M. Yan, J. Yu, and H. Liu**: Flexible electronics based on micro/nanostructured paper. *Adv. Mater.* **30**, 1801588 (2018).
22. **Y. Yang, Q. Huang, G.F. Payne, R. Sun, and X. Wang**: A highly conductive, pliable and foldable Cu/cellulose paper electrode enabled by controlled deposition of copper nanoparticles. *Nanoscale* **11**, 725 (2019).
23. **P. Yu, W. Fu, Q. Zeng, J. Lin, C. Yan, Z. Lai, B. Tang, K. Suenaga, H. Zhang, and Z. Liu**: Controllable synthesis of atomically thin type-II weyl semimetal WTe_2 nanosheets: An advanced electrode material for all-solid-state flexible supercapacitors. *Adv. Mater.* **29**, 1701909 (2017).
24. **X.M. Luo, X.F. Zhu, and G.P. Zhang**: Nanotwin-assisted grain growth in nanocrystalline gold films under cyclic loading. *Nat. Commun.* **5**, 3021 (2014).
25. **H.Y. Wan, X.M. Luo, X. Li, W. Liu, and G.P. Zhang**: Nanotwin-enhanced fatigue resistance of ultrathin Ag films for flexible electronics applications. *Mater. Sci. Eng. A* **676**, 421 (2016).
26. **B. Zhang, T.Y. Xiao, X.M. Luo, X.F. Zhu, and G.P. Zhang**: Enhancing fatigue cracking resistance of nanocrystalline Cu films on a flexible substrate. *Mater. Sci. Eng. A* **627**, 61 (2015).
27. **J. Yun**: Ultrathin metal films for transparent electrodes of flexible optoelectronic devices. *Adv. Funct. Mater.* **27**, 1606641 (2017).
28. **M.D.S.L. Wimalananda, J-K. Kim, and J-M. Lee**: Toward the ultra-transparent electrode by using patterned silver nanowire and graphene layered material. *Carbon* **125**, 9 (2017).
29. **C-A. Tseng, C-C. Chen, R.K. Ulaganathan, C-P. Lee, H-C. Chiang, C-F. Chang, and Y-T. Chen**: One-step synthesis of antioxidative graphene-wrapped copper nanoparticles on flexible substrates for electronic and electrocatalytic applications. *ACS Appl. Mater. Interfaces* **9**, 25067 (2017).
30. **C. Hwang, W-J. Song, J-G. Han, S. Bae, G. Song, N-S. Choi, S. Park, and H-K. Song**: Foldable electrode architectures based on silver-nanowire-wound or carbon-nanotube-webbed micrometer-scale fibers of polyethylene terephthalate mats for flexible lithium-ion batteries. *Adv. Mater.* **30**, 1705445 (2018).
31. **H-G. Wang, W. Li, D-P. Liu, X-L. Feng, J. Wang, X-Y. Yang, X-b. Zhang, Y. Zhu, and Y. Zhang**: Flexible electrodes for sodium-ion batteries: Recent progress and perspectives. *Adv. Mater.* **29**, 1703012 (2017).
32. **A. Kumar and C. Zhou**: The race to replace tin-doped indium oxide: Which material will win? *ACS Nano* **4**, 11 (2010).
33. **J-L. Wang, M. Hassan, J-W. Liu, and S-H. Yu**: Nanowire assemblies for flexible electronic devices: Recent advances and perspectives. *Adv. Mater.* **30**, 1803430 (2018).
34. **G.P. Zhang, K.H. Sun, B. Zhang, J. Gong, C. Sun, and Z.G. Wang**: Tensile and fatigue strength of ultrathin copper films. *Mater. Sci. Eng. A* **483–484**, 387 (2008).
35. **G.P. Zhang, C.A. Volkert, R. Schwaiger, P. Wellner, E. Arzt, and O. Kraft**: Length-scale-controlled fatigue mechanisms in thin copper films. *Acta Mater.* **54**, 3127 (2006).
36. **H.S. Liu, B. Zhang, and G.P. Zhang**: Delaying premature local necking of high-strength Cu: A potential way to enhance plasticity. *Scr. Mater.* **64**, 13 (2011).
37. **C. Lee, X. Wei, J.W. Kysar, and J. Hone**: Measurement of the elastic properties and intrinsic strength of monolayer graphene. *Science* **321**, 385 (2008).
38. **Y. Kim, J. Lee, M.S. Yeom, J.W. Shin, H. Kim, Y. Cui, J.W. Kysar, J. Hone, Y. Jung, S. Jeon, and S.M. Han**: Strengthening effect of single-atomic-layer graphene in metal-graphene nanolayered composites. *Nat. Commun.* **4**, 2114 (2013).
39. **S.H. Song, K.H. Park, B.H. Kim, Y.W. Choi, G.H. Jun, D.J. Lee, B.S. Kong, K.W. Paik, and S. Jeon**: Enhanced thermal conductivity of epoxy-graphene composites by using non-oxidized graphene flakes with non-covalent functionalization. *Adv. Mater.* **25**, 732 (2013).
40. **S.J. Kim, D.H. Shin, Y.S. Choi, H. Rho, M. Park, B.J. Moon, Y. Kim, S.K. Lee, D.S. Lee, T.W. Kim, S.H. Lee, K.S. Kim, B.H. Hong, and S. Bae**: Ultrastrong graphene–copper core–shell wires for high-performance electrical cables. *ACS Nano* **12**, 2803 (2018).
41. **M. Cao, D-B. Xiong, Z. Tan, G. Ji, B. Amin-Ahmadi, Q. Guo, G. Fan, C. Guo, Z. Li, and D. Zhang**: Aligning graphene in bulk copper: Nacre-inspired nanolaminated architecture coupled with in situ processing for enhanced mechanical properties and high electrical conductivity. *Carbon* **117**, 65 (2017).
42. **J. Hwang, T. Yoon, S.H. Jin, J. Lee, T.S. Kim, S.H. Hong, and S. Jeon**: Enhanced mechanical properties of graphene/copper nanocomposites using a molecular-level mixing process. *Adv. Mater.* **25**, 6724 (2013).

https://doi.org/10.1557/jmr.2019.290 Published online by Cambridge University Press

© Materials Research Society 2019

43. **Z. Yang, L. Wang, Z. Shi, M. Wang, Y. Cui, B. Wei, S. Xu, Y. Zhu, and W. Fei**: Preparation mechanism of hierarchical layered structure of graphene/copper composite with ultrahigh tensile strength. *Carbon* **127**, 329 (2018).
44. **R. Jiang, X. Zhou, and Z. Liu**: Electroless Ni-plated graphene for tensile strength enhancement of copper. *Mater. Sci. Eng. A* **679**, 323 (2017).
45. **F. Chen, J. Ying, Y. Wang, S. Du, Z. Liu, and Q. Huang**: Effects of graphene content on the microstructure and properties of copper matrix composites. *Carbon* **96**, 836 (2016).
46. **Y. Tang, X. Yang, R. Wang, and M. Li**: Enhancement of the mechanical properties of graphene–copper composites with graphene–nickel hybrids. *Mater. Sci. Eng. A* **599**, 247 (2014).
47. **W.J. Kim, T.J. Lee, and S.H. Han**: Multi-layer graphene/copper composites: Preparation using high-ratio differential speed rolling, microstructure and mechanical properties. *Carbon* **69**, 55 (2014).
48. **Z. Ren, N. Meng, K. Shehzad, Y. Xu, S. Qu, B. Yu, and J.K. Luo**: Mechanical properties of nickel–graphene composites synthesized by electrochemical deposition. *Nanotechnology* **26**, 065706 (2015).
49. **J. Wang, Z. Li, G. Fan, H. Pan, Z. Chen, and D. Zhang**: Reinforcement with graphene nanosheets in aluminum matrix composites. *Scr. Mater.* **66**, 594 (2012).
50. **Z. Li, G. Fan, Z. Tan, Q. Guo, D. Xiong, Y. Su, Z. Li, and D. Zhang**: Uniform dispersion of graphene oxide in aluminum powder by direct electrostatic adsorption for fabrication of graphene/aluminum composites. *Nanotechnology* **25**, 325601 (2014).
51. **X. Li, W. Cai, J. An, S. Kim, J. Nah, D. Yang, R. Piner, A. Velamakanni, I. Jung, E. Tutuc, S.K. Banerjee, L. Colombo, and R.S. Ruoff**: Large-area synthesis of high-quality and uniform graphene films on copper foils. *Science* **324**, 1312 (2009).
52. **B. Zhang, W.H. Lee, R. Piner, I. Kholmanov, Y. Wu, H. Li, H. Ji, and R.S. Ruoff**: Low-temperature chemical vapor deposition growth of graphene from toluene on electropolished copper foils. *ACS Nano* **6**, 2471 (2012).
53. **X. Li, L. Colombo, and R.S. Ruoff**: Synthesis of graphene films on copper foils by chemical vapor deposition. *Adv. Mater.* **28**, 6247 (2016).
54. **A.C. Ferrari, J.C. Meyer, V. Scardaci, C. Casiraghi, M. Lazzeri, F. Mauri, S. Piscanec, D. Jiang, K.S. Novoselov, S. Roth, and A.K. Geim**: Raman spectrum of graphene and graphene layers. *Phys. Rev. Lett.* **97**, 187401 (2006).
55. **Z.H. Ni, H.M. Wang, J. Kasim, H.M. Fan, T. Yu, Y.H. Wu, Y.P. Feng, and Z.X. Shen**: Graphene thickness determination using reflection and contrast spectroscopy. *Nano Lett.* **7**, 2758 (2007).
56. **K. Chu, F. Wang, Y-b. Li, X-h. Wang, D-j. Huang, and Z-r. Geng**: Interface and mechanical/thermal properties of graphene/copper composite with Mo_2C nanoparticles grown on graphene. *Composites, Part A* **109**, 267 (2018).
57. **A. Nieto, A. Bisht, D. Lahiri, C. Zhang, and A. Agarwal**: Graphene reinforced metal and ceramic matrix composites: A review. *Int. Mater. Rev.* **62**, 241 (2016).
58. **D-B. Xiong, M. Cao, Q. Guo, Z. Tan, G. Fan, Z. Li, and D. Zhang**: Graphene-and-copper artificial nacre fabricated by a preform impregnation process: Bioinspired strategy for strengthening-toughening of metal matrix composite. *Acs Nano* **9**, 6934 (2015).
59. **M. Li, H. Che, X. Liu, S. Liang, and H. Xie**: Highly enhanced mechanical properties in Cu matrix composites reinforced with graphene decorated metallic nanoparticles. *J. Mater. Sci.* **49**, 3725 (2014).
60. **X. Zhu, Y. Zhao, L. Ma, G. Zhang, W. Ren, X. Peng, N. Hu, L. Rintoul, J.M. Bell, and C. Yan**: Graphene coating makes copper more resistant to plastic deformation. *Compos. Commun.* **12**, 106 (2019).
61. **Y. Zhao, X. Peng, T. Fu, X. Zhu, N. Hu, and C. Yan**: Strengthening mechanisms of graphene coated copper under nanoindentation. *Comput. Mater. Sci.* **144**, 42 (2018).
62. **R.R. Nair, P. Blake, A.N. Grigorenko, K.S. Novoselov, T.J. Booth, T. Stauber, N.M.R. Peres, and A.K. Geim**: Fine structure constant defines visual transparency of graphene. *Science* **320**, 1308 (2008).
63. **J.L. Ni, X.F. Zhu, Z.L. Pei, J. Gong, C. Sun, and G.P. Zhang**: Comparative investigation of fracture behaviour of aluminium-doped ZnO films on a flexible substrate. *J. Phys. D: Appl. Phys.* **42**, 175404 (2009).
64. **X. Zhu, B. Zhang, J. Gao, and G. Zhang**: Evaluation of the crack-initiation strain of a Cu–Ni multilayer on a flexible substrate. *Scr. Mater.* **60**, 178 (2009).
65. **C. Zhang, C. Lu, L. Pei, J. Li, R. Wang, and K. Tieu**: The negative Poisson's ratio and strengthening mechanism of nanolayered graphene/Cu composites. *Carbon* **143**, 125 (2019).
66. **J. Wang, X. Zhang, N. Zhao, and C. He**: In situ synthesis of copper-modified graphene-reinforced aluminum nanocomposites with balanced strength and ductility. *J. Mater. Sci.* **54**, 5498 (2018).
67. **S. Chen, Q. Wu, C. Mishra, J. Kang, H. Zhang, K. Cho, W. Cai, A.A. Balandin, and R.S. Ruoff**: Thermal conductivity of isotopically modified graphene. *Nat. Mater.* **11**, 203 (2012).
68. **Y.J. Yang, B. Zhang, H.F. Tan, X.M. Luo, and G.P. Zhang**: Fatigue and fracture reliability of shell-mimetic PE/TiO_2 nanolayered composites. *Adv. Eng. Mater.* **19**, 1700246 (2017).
69. **C. Dai, X. Zhu, and G. Zhang**: Tensile and fatigue properties of free-standing Cu foils. *J. Mater. Sci. Technol.* **25**, 721 (2009).
70. **Y-J. Yang, B. Zhang, H-Y. Wan, and G-P. Zhang**: Optimizing fatigue performance of nacre-mimetic PE/TiO_2 nanolayered composites by tailoring thickness ratio. *J. Mater. Res.* **33**, 1543 (2018).

https://doi.org/10.1557/jmr.2019.290 Published online by Cambridge University Press

© Materials Research Society 2019